Ultrasound in Med. & Biol., Vol. 34, No. 10, pp. 1651–1665, 2008

0301-5629/08/$–see front matter

ELSEVIER

doi:10.1016/j.ultrasmedbio.2008.03.011

● *Original Contribution*

A PASSIVE ACOUSTIC DEVICE FOR REAL-TIME MONITORING OF THE EFFICACY OF SHOCKWAVE LITHOTRIPSY TREATMENT

T. G. LEIGHTON,* F. FEDELE,† A. J. COLEMAN,† C. MCCARTHY,† S. RYVES,‡ A. M. HURRELL,§ A. DE STEFANO,¶ and P. R. WHITE*

*Institute of Sound and Vibration Research, University of Southampton, Southampton; †Medical Physics Department, Guy's and St. Thomas' NHS Foundation Trust, London; ‡Stone Unit, Day Surgery Department, Guy's and St. Thomas' NHS Foundation Trust, London; §Precision Acoustics Ltd., Dorset; and ¶Radiological Science Group, Medical Physics Department, St. Mary's Hospital, Hampshire, UK

(*Received* 11 *October* 2007; *revised* 24 *February* 2008; *in final form* 10 *March* 2008)

Abstract—Extracorporeal shockwave lithotripsy (ESWL) is the preferred modality for the treatment of renal and ureteric stone disease. Currently X-ray or ultrasound B-scan imaging are used to locate the stone and to check that it remains targeted at the focus of the lithotripter during treatment. Neither imaging modality is particularly effective in allowing the efficacy of treatment to be judged during the treatment session. A new device is described that, when placed on the patient's skin, can passively monitor the acoustic signals that propagate through the body after each lithotripter shock, and which can provide useful information on the effectiveness of targeting. These acoustic time histories are analyzed in real time to extract the two main characteristic peak amplitudes (m_1 and m_2) and the time between these peaks (t_c). A set of rules based on the acoustic parameters was developed during a clinical study in which a complete set of acoustic and clinical data was obtained for 30 of the 118 subjects recruited. The rules, which complied with earlier computational fluid dynamics (CFD) modeling and *in vitro* tests, allow each shock to be classified as "effective" or "ineffective." These clinically-derived rules were then applied in a second clinical study in which complete datasets were obtained for 49 of the 85 subjects recruited. This second clinical study demonstrated almost perfect agreement (kappa = 0.94) between the number of successful treatments, defined as >50% fragmentation as determined by X-ray at the follow-up appointment, and a device-derived global treatment score, TS_0, a figure derived from the total number of effective shocks in any treatment. The acoustic system is shown to provide a test of the success of the treatment that has a sensitivity of 91.7% and a specificity of 100%. In addition to the predictive capability, the device provides valuable real-time feedback to the lithotripter operator by indicating the effectiveness of each shock, plus an indication *TS(t)* of the cumulative effectiveness of the shocks given so far in any treatment, and trends in key parameters. This feedback would allow targeting adjustments to be made during treatment. An example is given of its application to mistargeting because of respiration. (E-mail: tgl@soton.ac.uk) **© 2008 World Federation for Ultrasound in Medicine & Biology.**

Key Words: **Lithotripsy, Cavitation, Computational fluid dynamics, Kidney stone fragmentation, Bioeffect, Effective shock, ESWL, Passive acoustic sensor.**

INTRODUCTION

Extracorporeal shockwave lithotripsy (ESWL) was introduced in the 1980s and has become the preferred modality for the treatment of renal and ureteric stone disease. The treatment involves focusing several thousand acoustic shockwaves on the stone to generate stone fragments that are small enough to be passed naturally from the body, or, more effectively, dissolved by drugs (Chaussy and Schmiedt 1983). Technical improvements in the second and third-generation machines have been associated with reduced anesthesia requirements, increased functionality and greater user convenience, although these improvements have been associated with generally inferior stone-free rates when compared with the first generation Dornier HM3 (Dornier MedTech Europe GmbH, Wessling, Germany) (Madaan et al. 2007). Typically, 30–50% of patients need retreatment with ESWL

To accompany this paper, a web page with a movie of the software running is available at: http://www.isvr.soton.ac.uk/fdag/Litho_07/litho_07(main).htm.

Video Clips cited in this article can also be found online at: http://www.umbjournal.org.

Address correspondence to: Prof. Timothy G. Leighton, Institute of Sound and Vibration Research, University of Southampton, Highfield, Southampton S017 1BJ, United Kingdom. E-mail: tgl@soton.ac.uk

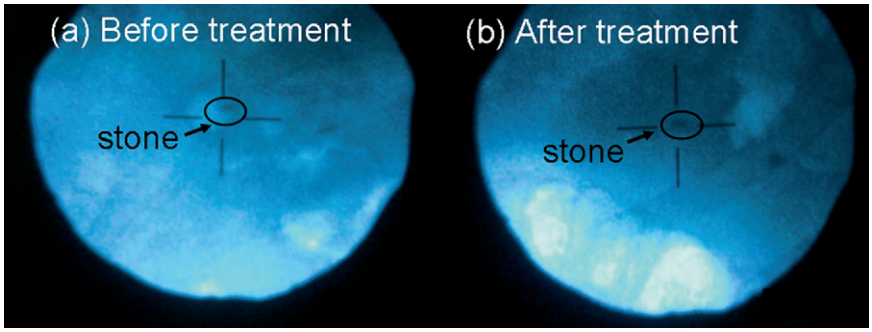

Fig. 1. X-ray image of a stone (a) before and (b) immediately after ESWL.

(Tan et al. 2002; Papadoukakis et al. 2006), with some undergoing more than three treatments for the same stone (Auge and Preminger 2002; Lingeman et al. 1986; Tolley and Downey 1999). Retreatment is a useful option but involves additional morbidity because of, among other things, the bruising of tissue caused by the passage of the shockwave (Skolarikos et al. 2006).

A range of physical factors has been found to influence the stone-free rate and morbidity associated with ESWL treatment. These include the size of stone, its location and density, the anatomical position and such factors as the body mass index of the patient (Delakas et al. 2003; Gomha 2004; Lingeman et al. 1986; Papadoukakis et al. 2006). Few studies, however, have examined the influence of the actions of the ESWL operator. The maintenance of accurate targeting throughout the treatment, for example, is under operator control using ultrasound or X-ray imaging systems (Fig. 1a) and can be expected strongly to influence treatment effectiveness (Warner et al. 1988). The operator also selects the shockwave strength setting, typically using the highest setting compatible with the level of pain tolerated by the patient (Auge and Preminger 2002). Ideally, the operator would also have a role in limiting the morbidity associated with shockwave exposure (Madaan et al. 2007), for example by terminating the treatment when the stone has fragmented fully. In practice, the current imaging systems are largely inadequate for indicating when stone fragmentation is complete (Schmitt et al. 1990; Fig. 1b), and the strategy adopted almost universally by ESWL operators is to deliver a predefined number of shockwaves (typically around 3,000). Finally, the operator has a significant role in minimizing the ionizing radiation exposure by restricting the fluoroscopy exposure time and number of spot films within the constraint of achieving accurate shockwave targeting of the stone (Sandilos et al. 2006). More information on treatment progress and targeting during clinical ESWL may allow the operator to exercise greater control over many of the factors that influence retreatment rate and morbidity.

This article describes a new passive device that provides the ESWL operator with information on the maintenance of accurate targeting of the stone and a measure of the effectiveness of the treatment. The device consists of a passive acoustic sensor placed on the patient during treatment that monitors the acoustic signal scattered when the shockwave impinges on the stone and surrounding tissues. This signal is processed in real time to provide easily interpreted visual cues to the ESWL operator. These cues can be used to inform decisions related to the need for retargeting and to the ongoing effectiveness of the treatment. This paper reports on a clinical study, in which the performance of the device has been compared with measures of the degree of stone fragmentation obtained from pre and post-ESWL X-ray films interpreted by clinical staff immediately after treatment, and at the follow-up appointment three weeks later.

The development of the clinical system described in this paper has previously proceeded through initial computational fluid dynamics (CFD) studies (Leighton 2004; Turangan et al. 2008) and an *in vitro* testing phase (Leighton et al. 2004; Fedele et al. 2004a, 2004b, 2004c, 2004d). These preparatory studies were conducted to characterize the acoustic emission signal and gauge which parameters could be extracted from it to provide an assessment of the treatment (Cunningham et al. 2001; Fedele et al. 2004a, 2004b, 2004c, 2004d; Leighton et al. 2005). These *in vitro* studies progressed to the design of the device and the manufacture of a prototype, in collaboration with a UK company (Precision Acoustics Ltd., Dorset). This paper reports on the clinical testing of the device on patients, 17 years after it was originally conceived.

Theory

Bubble dynamics simulations. A physical interpretation of the acoustic signal generated by shockwave interactions with tissues and stones during ESWL forms

the basis for the clinical use of the device described in this paper. Collaboration between academia (Leighton 1994) and the health service (Coleman et al. 1992, 1993) led to the initial identification of an acoustic signal generated during lithotripsy that appeared to have potential clinical value. This signal is, specifically, a two-peak time history with a characteristic time interval between the peaks (which we will call t_c, noting that the precise method of calculating this has changed over the years—described later in this manuscript). By comparing acoustic and sonoluminescent emissions with the predictions of the Gilmore equation (Fig. 2), Coleman and Leighton were able to identify the two peaks with the pressure signals generated by the collapse and rebounds of cavitation bubbles. Furthermore, they were able to relate the interval between these peaks (t_c) with key characteristics of the event, such as the initial bubble size and the magnitude of the lithotripter pulse. In the years since its discovery, several laboratories around the world have found ingenious ways to exploit this two-peak structure to characterize responses as a result of lithotripsy (Bailey et al. 2005; Cleveland et al. 2000; Matula et al. 2002; Zhong et al. 1997; Xu et al. 2007).

An improved theoretical understanding of the two-peak signal has been provided by recent complementary work (Turangan et al. 2008) undertaken in parallel with the present study. The goal of this work was to extend current simulation capabilities to allow the incorporation of liquid compressibility into the interaction of the cavity with the stone. This opens up the possibility of simulating, for the first time, an ESWL-induced blast wave (the GPa pressures in which can greatly exceed those in the lithotripter pulse, which suggests an *a priori* importance to stone fragmentation (see Fig. 23 of Leighton 2004)), the resulting stresses within the stone or other solids in the presence of cavitation (Fig. 3) and the generation of the far-field pressure signature used in this paper.

This complementary study (Turangan et al. 2008) represents a major advance over current modeling capabilities, because the Gilmore equation (Fig. 2) assumes that the bubble remains spherical, and those current approaches that allow departures from bubble sphericity are limited by the assumption of liquid incompressibility and thus cannot predict the blast wave (Blake et al. 1997; Ding and Gracewski 1996; Fong et al. 2006; Klaseboer et al. 2006). The complementary publication on this second theme (Turangan et al. 2008) details the interactions of single bubbles with solids in soft tissue and liquid, and the corresponding stresses and pressure and likelihood of material failure are estimated. Future publications will detail the cloud cavitation and far-field signature calculations that informed the design of the sensor used in the current study.

The pressure waveform generated during clinical

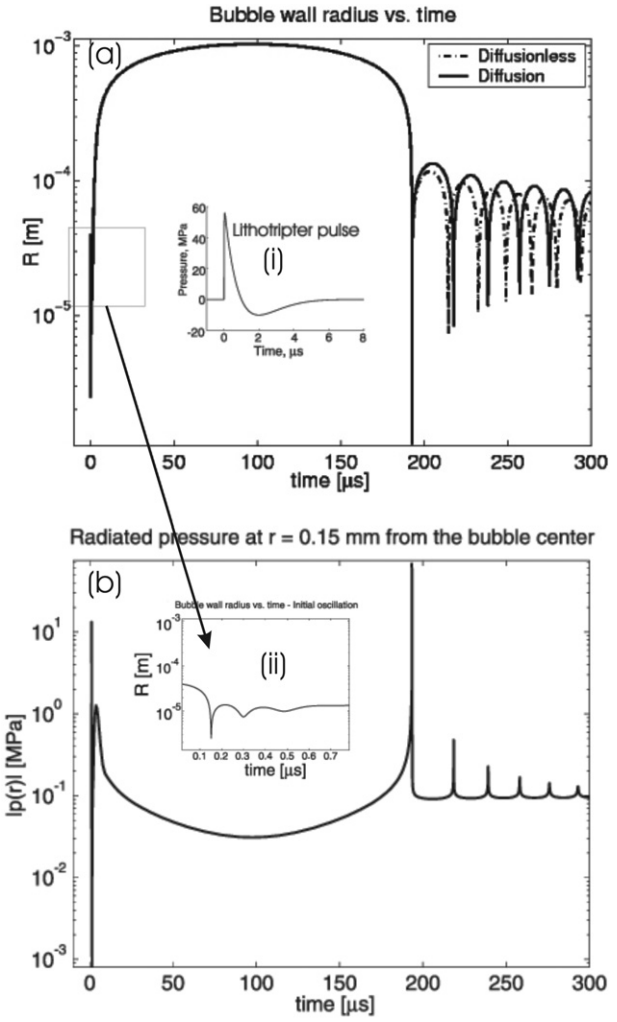

Fig. 2. An air bubble of initial radius 40 μm in water is subjected in the free field to the lithotripter pulse shown in inset (i) (Peak positive pressure = 56 MPa; Peak negative pressure = −10 MPa). (a) The bubble radius against time is shown, as predicted by the Gilmore model, with (solid line) and without (dashed line) mass flux across the bubble wall. Inset (ii) shows the micro-rebounds that are visible in the fine detail of the collapse, which occurs around $t = 0$. Similar features are seen in the CFD predictions (Turangan et al. 2008). (b) On a common time axis with (a) and for the same bubble collapse, the pressure that would be measured 1.5 mm away from the bubble center is shown. Two main emissions (at $t \approx 0$ μs and at $t \approx$ 190 μs) are associated with rebounds in (a), subsequent emissions being smaller. The overall effect of such pairs of emissions from the collapse of a cloud of bubbles was identified as demarcating the interval t_c in the early 1990s (Coleman et al. 1992, 1993; Leighton 1994). Figure courtesy of AR Jamaluddin, CK Turangan, GJ Ball and TG Leighton.

ESWL is detected using a sensor placed on the skin. It is then analyzed to determine to what extent the time history can be interpreted as a double-peak feature. This double-peak structure is not always obvious from visual

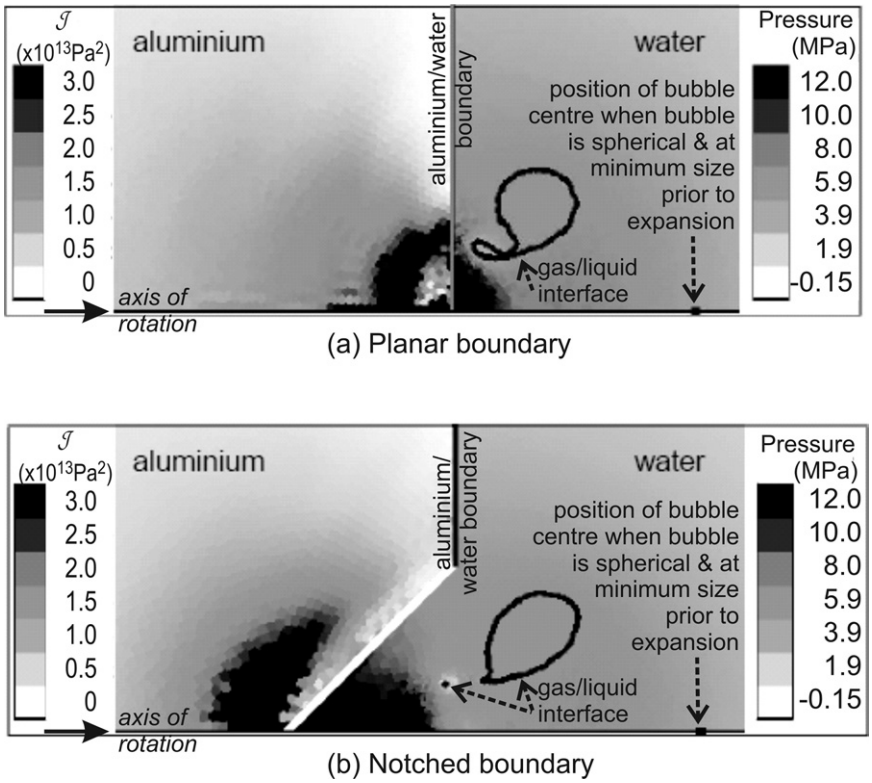

Fig. 3. The bubble shapes and the distributions of pressure and stress are indicated for a bubble near planar and notched aluminium walls, after a high-speed jet has passed through the bubble (a situation that can only be modeled with accuracy by a simulation that includes liquid compressibility). Although not an exact match, in the context of this paper this scenario resembles the situation approximately at the time associated with the generation of the signal m_2. The base of each image is an axis of rotational symmetry. The right half of each image maps the distribution of pressure in the liquid (in MPa). The left half of each image maps a parameter [$\mathcal{J}$, units Pa^2] that is equal to twice the second invariant of stress. Elastic–plastic yield will occur in aluminium when the value of $\mathcal{J}$ exceeds 6×10^{16} Pa^2. The upper image shows the case when the aluminium surface is planar, and the lower image shows the case when the aluminium contains a conical notch: the presence of the notch concentrates stress at the crack tip. Current computational resources are not sufficient to run this CFD code from the initial impact of the lithotripter shock with the bubble, for several hundred microseconds up until the generation of the m_2 signal. Shortcuts have to be found, such as linking the two during the prolonged expansion *via* the Gilmore model or a boundary–integral method (Turangan et al. 2008). In the case shown here, the analogy is made by assuming that mass flux has increased the effective size of the bubble such that, if the mass of gas in the bubble shown in Fig. 3 were contained in a spherical, intact bubble at room temperature and pressure, its radius would be 1.7 mm. This is done by starting the CFD 134 μs earlier than the moment shown in Fig. 3, with the initial conditions that the bubble is intact, spherical, with stationary walls and that its centre was located at the position indicated in the figure (the bubble contained air at 81.06 MPa and 1252 K, in water at room temperature and pressure, and its center was 1.44 mm from the plane aluminium/water boundary). These initial conditions cause the bubble to expand (akin to laser-generation of a bubble but, in the context of this paper, a situation resembling the conditions shortly after the generation of the signal m_1). The maximum radius attained during bubble expansion is 1.8 mm, after which the collapse shown in Fig. 3 occurs. When the bubble was stationary before expansion, it was assumed to be surrounded by water in which the pressure, temperature and density were uniform at 101.325 kPa, 288.15 K and 1000 kg m^{-3}, respectively (note that the lithotripter shockwave would have propagated away from the bubble at this time; see the movie at: http://www.isvr.soton.ac.uk/fdag/Litho_07/litho_07(main).htm). For full details of this case, see Turangan et al. (2008).

inspection of the time history, but can be revealed by processing described later (Fig. 4). The first peak (which is labeled with amplitude m_1 in Fig. 4a), is produced at the time when the shock initially interacts with the stone. This time marks the generation of a range of pressure features, including a reflection of the incident lithotripter pulse from the stone and the pressure pulse emitted by the first rebound of the collapsing bubble. A reduction in m_1 might, therefore, be interpreted as misalignment between the stone and the focus of the lithotripter, because there is a failure of the stone to generate a strong reflection of the incident shock. The subsequent pressure pro-

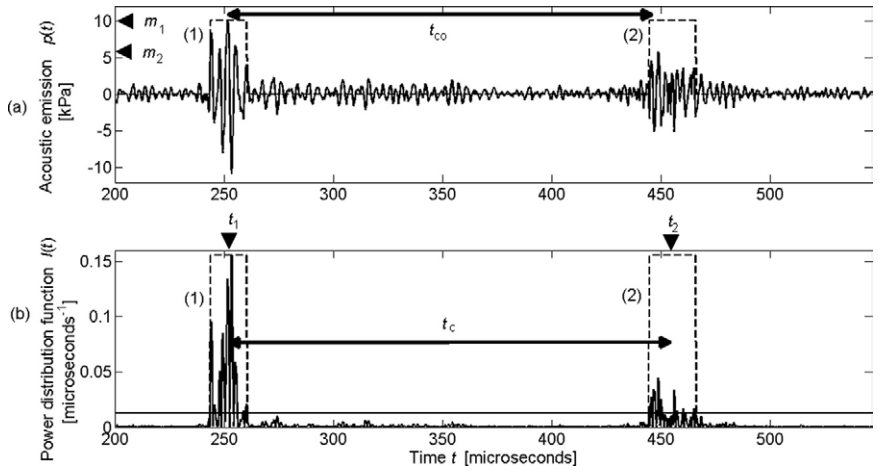

Fig. 4. (a) A sample pressure waveform obtained with the PAS during clinical ESWL (the datum of time corresponds to the electrical triggering of the lithotripter). (b) The power distribution function (see eqn (1)) of the data shown in (a) is used to detect the two bursts, which are labeled (1) and (2). The solid line indicates the threshold used by the detection algorithm. Software is used to extract the maximum amplitude of the first and second bursts (m_1 = 10 kPa and m_2 = 5.8 kPa), the central time of the first and second bursts (t_1 = 251 μs and t_2 = 453 μs) and the collapse time (t_c = 202 μs). Also shown for comparison is the more commonly defined collapse time (t_{co} = 197 μs), which is the separation of the two highest peaks. This was not found to be a robust measure for automated analysis (in this figure they agree to within 2.5%, but the discrepancy increases as the symmetry of the bursts decreases). The dotted line demarcates the regions identified as (1) first burst and (2) second burst.

file is complicated by the interaction of the pressure field in the tissue, any cavitation and the pressure field within the stone (Chitnis and Cleveland 2006; Cleveland et al. 1998, 2005; Leighton, 2004; Owen et al. 2007; Pishchalnikov et al. 2003; Turangan et al. 2008; Xi 2000; Xi and Zhong 2001; Zhong and Zhou 2001; Zhong et al. 1993; Zhu et al. 2002). However, in the early stages of this work, a simple and useful model interpretation was provided by comparing the passive emissions with the predictions of the Gilmore model for the behavior of a single gas bubble under such conditions (Coleman et al. 1992; Cunningham et al. 2001; Leighton 1994). Both experiment (Leighton et al. 2000; Leighton 2007) and simulation (Leighton 2004; Turangan et al. 2008) have shown that the actual cavitational dynamics may involve complicating features not included in the Gilmore model. However, such studies have also shown how useful the explanations from simple models can be. This is because, if interpreted with caution, the ensemble effect can produce features similar to those generated by the simple models. An example of this occurs if the fragmentation of a collapsing bubble is reversed by the subsequent coalescence of the fragments during the subsequent expansion phase (Leighton et al. 2000). Based on these considerations of bubble dynamics, a simple explanation of Fig. 4 is that the bubbles undertake a prolonged expansion phase through much of the interval t_c. This expansion phase is terminated by cavitational collapse and a rebound, such that the peak m_2 corresponds to a pressure wave generated at that rebound. Hence, a long interval t_c might be interpreted as evidence of pronounced inertial cavitation provided that it is clearly terminated by a large second peak (with strong m_2).

Physical interpretation. The general principles outlined in the preceding section can be used to provide warning of a number of conditions unfavorable to effective stone fragmentation:

(i) Poor targeting would cause a low value of m_1
(ii) Weak cavitation would cause a low value of m_2
(iii) Weak cavitation would cause a small value for t_c

Clearly, the physical interpretation of these parameters suggests that they are not entirely independent. The value of m_1, for example, may in practice correlate to a greater or lesser extent with the value of m_2. Similarly, m_2 and t_c can be expected to be correlated to some extent. In the study presented here, the possible lack of independence of these parameters may enhance the robustness of measurement techniques. The important hypothesis on which the study is based is that these parameters have a useful clinical interpretation in terms of treatment efficacy that can be tested in the clinic by comparison with the clinical outcome of the treatment. From previous *in vitro* studies, for example, it is found that a possible criterion for determining if a shock had been "effective" in targeting and fragmenting the stone could be based on the requirement that $m_2/m_1 > 0.4$ and $t_c \sim 300$ μs (Fedele 2008). Phase 1 of the clinical studies

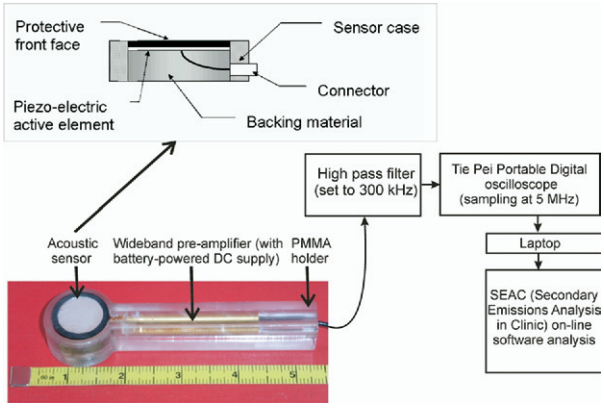

Fig. 5. Schematic of the apparatus. The signal from the transducer and preamplifier (manufactured by Precision Acoustics, Ltd.) is high-pass filtered to reduce noise and captured by a portable oscilloscope before being analyzed on the laptop using the SEAC online software.

described in this paper has examined the validity and application of these "rules" to the *in vivo* tests.

METHODS

The study involved the development of an acoustic sensor, signal processing software and an operator interface providing real-time data to the ESWL operator. This system was then developed and evaluated in two separate clinical studies. The first clinical study (phase 1) was used to gain experience with the system and to compare the value of the acoustic signal parameters with the clinical outcome of the treatment. The results of phase 1 allowed a set of semi-empirical rules to be devised that were then incorporated into software (these rules were adaptations, based on the clinical experience, of the rules devised from the *in vitro* tests, as discussed previously). The role of this software is to convert acoustic observables into parameters more readily interpreted, in terms that are valuable for clinical decision-making during the treatment. In the second clinical study (phase 2), the clinically adapted system and software were evaluated against clinical judgments made from X-ray images. Details of the hardware, software processing and two clinical studies are given in the following sections.

Description of hardware. The measurement hardware comprises two distinct components: a dedicated passive acoustic sensor (PAS) and the signal-conditioning electronics. A block diagram of the hardware can be found in Fig. 5, which includes an inset diagram of the sensor. The PAS has a piezo-polymer element of 18-mm diameter located in a holder with an outer diameter of 25 mm. The piezoelectric layer is protected by a biocompatible front face with acoustic properties optimized to ensure maximum acoustic sensitivity. The rear surface of the sensor is filled with a backing material to prevent internal reverberations. The voltage waveform generated is extracted by means of a wide bandwidth radiofrequency connector mounted in the side wall of the sensor case. With the exception of the connector and the wires attached to it, all components of the acoustic sensor are polymeric. The resulting PAS has a total weight of 7*g*.

To preserve signal integrity, the output of the acoustic sensor is connected directly to a wideband preamplifier (with direct current power supply) that buffers the electrical impedance to 50 Ohms (HP1, Precision Acoustics Ltd.). The part of the PAS applied to the patient forms a potentially conductive contact and is classified for electrical safety purposes in the same way as an electrocardiogram electrode under the international electrical safety standards for medical devices (IEC 1988).

Feature extraction processing. A sample pressure waveform obtained using the PAS in the clinic is shown in Fig. 4a, which is characteristic of the double peak or "two burst" signal reported widely in studies of acoustic emission at the focus of a lithotripter. A block diagram of the algorithm used to extract features from waveforms of this type is shown in Fig. 6. The algorithm contains three key steps: first, the detection of the two bursts; second, the analysis of the acoustic parameters asso-

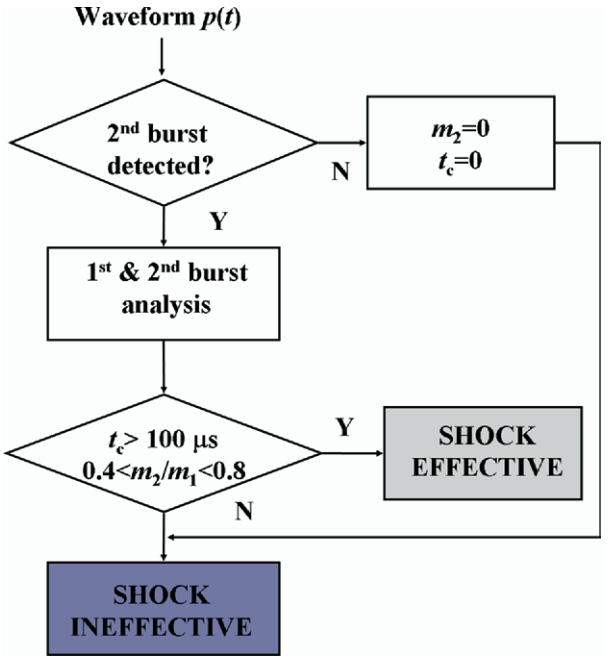

Fig. 6. A block diagram of the SEAC software. The detected acoustic emission is processed, making use of clinically-derived data on the acoustic parameters m_2/m_1 and t_c, to generate an indication to the operator of the effectiveness of a shock (the "rules" displayed in the lower diamond correspond to those determined by phase 1 for use in phase 2).

ciated with each burst; and third, the classification of each shock based on the clinically-derived rules defining "effectiveness."

The detection of the bursts involves an initial calculation of a power function $I(t)$ from the voltage waveform $p(t)$:

$$I(t) = \frac{p^2(t)}{\int p^2(t)dt} \quad (1)$$

where the integral is calculated over a time long enough to contain the whole signal (400 μs). A plot of $I(t)$ is shown in Fig. 4b. In this quadratic signal, the two bursts (which are those portions of the signal at highest powers $p^2(t)$) are emphasized above the noise level. In addition, the signal $I(t)$ is defined to have a unitary integral over the interval considered, so that it represents a distribution function of the power in that interval. The threshold is taken at the 96th percentile of $I(t)$ (Papoulis and Pillai 2001). The specific percentile was selected as the optimum by trial and error using a set of measured waveforms (Fedele 2008). The algorithm identifies the two bursts (Fig. 4) as the two regions of adjacent points that are above the threshold. A minimum separation time of 20 μs is imposed between the two regions, except for the special circumstance when the signal is such that a second burst cannot be detected above the noise, whereupon the algorithm allocates a conventional value of $t_c = 0$ and $m_2 = 0$ to the signal. We interpret a signal with $t_c = 0$ and $m_2 = 0$ as indicating "ineffective" targeting, although, of course, some such signals may originate from equipment-related effects such as poor acoustic coupling between the PAS or lithotripter and the skin.

Once the bursts have been identified, the peak values in each burst (m_1 and m_2) are noted. In addition, a single energy-weighted central time t_i is allocated to each of the two regions using:

$$t_i = \int_{t_{i,\min}}^{t_{i,\max}} tI_i(t)dt \quad (2)$$

where $i = 1,2$ indicates which burst is under consideration, and where $I_i(t)$ is the relative power distribution function of the i^{th} region. That is to say, $I_i(t)$ is calculated using eqn (1) but with the integration of the denominator occurring from $t_{i,\min}$ (the start time of the burst under consideration) to $t_{i,\max}$ (the end time of the burst under consideration). Having calculated t_1 and t_2 in this way, the interval t_c is found from $t_c = t_2 - t_1$. These parameters are shown in Fig. 4. This estimate of t_c used in the current investigation (Fedele et al. 2003, 2004a, 2004b, 2004c), differs from that introduced by the authors (Coleman et al. 1992, 1993; Leighton 1994), which is labeled as t_{co} in Fig. 4. The revised estimate, t_c, is valuable because it is robust and less dependent on noise. This interpretation of the signal in the time domain was found to be more functional *in vivo* than an earlier scheme based on a frequency domain interpretation, which nevertheless has proved to be useful *in vitro* (Fedele et al. 2004a, 2004b, 2004c, 2004d; Owen et al. 2007).

The display of results: Secondary Emissions Analysis in Clinic (SEAC) real-time display software. Figure 7 is a screen shot (see footnote on article's first page for URL) of the SEAC output, with dashed lines added to facilitate the explanation. These dashed lines divide the screen shot into boxes, numbered (1) to (5). The SEAC software allows storage of patient identification details (Box 1) and control of the waveform capture *via* oscilloscope settings (Box 2). Waveform acquisition is triggered from the electromagnetic pickup produced on the generation of each shock, and the "Analysis start time" slider in Box 2 ensured that there was sufficient delay after triggering to eliminate the electromagnetic signal from the analysis. The lithotripter source power level or setting is entered manually and displayed in Box 2 along with a virtual red/green "traffic light" indicator at the bottom right corner of Box 2. This light was updated after every shock to provide the ESWL operator with real-time feedback about whether the previous shock had been effective so that, *e.g.*, a sustained red display in this indicator could prompt the operator to consider retargeting the stone.

Box 3 in Fig. 7 was included to allow additional digital filtering of the data, either to improve the signal-to-noise ratio or to look only at specific frequency components. This option was disabled for the current study. Box 4 records a count of the number of shocks administered and information on software-equipment interfacing. A *Test On* button (in Box 4) allowed the software to run in test mode (*i.e.*, without saving any data), to check the appropriate settings to use for the specific treatment before starting the acquisition and storage of large quantities of data in the form of voltage waveforms for each shock. The *Start* button began the acquisition of data, and is replaced by a *Stop* button during acquisition.

A quantitative treatment score (TS_0) is shown in the pop-up window (Box 5). This score is based on the percentage of shocks that have been classified by the system as "effective," relative to the total number already fired. The conditions for a shock to be classified as "effective" were derived from the phase 1 clinical study described later (and shown in the lower diamond box of Fig. 6). In addition to these indicators, the graph on the lower left of the screen in Fig. 7 shows the waveform captured by the PAS from each shock. It provides a visual clue to the operator about the ongoing functioning of the acoustic system. The two graphs stacked one above another on the lower right of the screen in Fig. 7

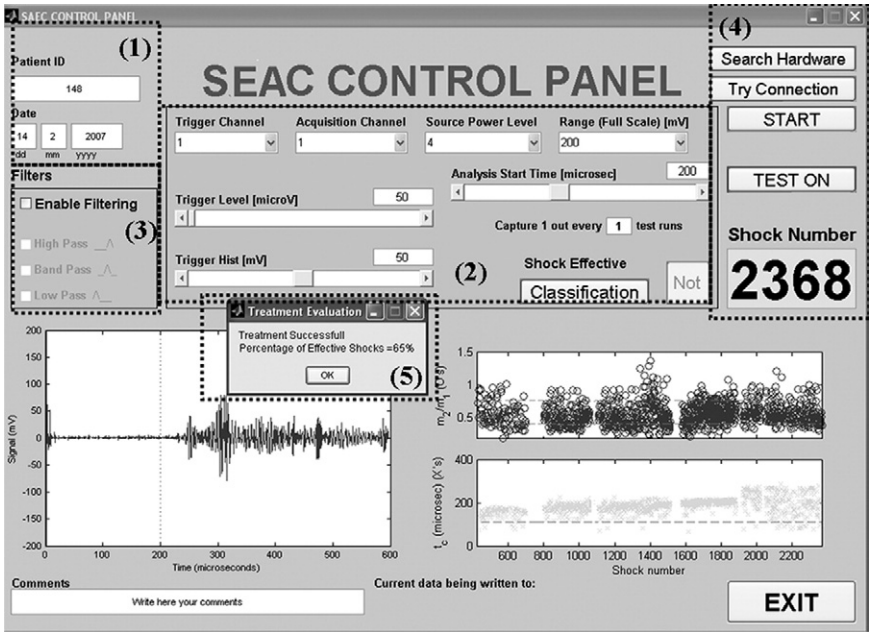

Fig. 7. A screenshot of the output of the SEAC software interface used by the ESWL operator during phase 2 of the project. The dotted lines demarcating numbered boxes have been added to identify areas in the display (see text for details). Box 5 gives an indication of the percentage of the 2,368 shocks given in this treatment that were effective at damaging the stone (TS_0). A score here of 65% indicates a successful treatment. The values of the acoustic parameters (m_2/m_1 and t_c) for each shock are shown in the graphs on the bottom right of the interface. There are, therefore, three primary outputs from SEAC: the treatment score TS_0 obtained at the end of the treatment; the cumulative ratio $TS(t)$ of effective shocks to the total number of shocks given from the start of the treatment to any point during it (which equals TS_0 at the end of treatment); and the red-green indicator light that provides feedback on the most recent shock. Trends in these are available (*e.g.*, *via* the two graphs on the bottom right of the screen).

plot the single-shock values of m_2/m_1 (upper panel, open circles) and t_c (lower panel, grey crosses) as a visual guide to trends in the effectiveness of a set of shocks.

Methodology. The two clinical studies reported in this paper were carried out by the Medical Physics Department at Guy's & St. Thomas' NHS Trust, London, on patients treated for stones either in the renal pelvis or the calicies on Storz Modulith SLX lithotripter (Storz Medical AG, Tägerwilen, Switzerland) located in the Stone Unit of the same hospital. The studies received ethics approval, and the first study (phase 1) commenced in April 2006 and, together with the phase 2 study, lasted 15 months. The scope of the ethics approval did not allow the ESWL operator to alter the treatments in any way in response to information provided by the SEAC display. The study aim was confined, therefore, to examining the correlation between the acoustic data and the clinical outcome. The object of the phase 1 study was to build on the *in vitro* and CFD results to finalize the rules for determining the effectiveness of each shock. In phase 2, these rules were implemented and the system was validated.

A total of 118 patients consented to take part in phase 1. Shock-by-shock sequences of acoustic data from the sensor were retained for the analysis of each treatment. A clinical follow-up three weeks after treatment was obtained for 67 of these subjects in phase 1. (Of the remainder, 18 subjects could not tolerate the procedure, for 3 patients the pre-treatment and post-treatment X-Rays were not of adequate quality for reporting [see caption to Fig. 8] and in 30 further cases the patients failed to return for the follow-up appointment.) The acoustic data from these 67 subjects were examined, and a further 37 of these subjects were excluded on the basis that the recorded sequences of the patient in question represented less than 30% of the shocks administered to that patient during the treatment session (phase 1 was used not only to test the "rules" for the diagnosis, but also to test and enhance the ruggedness of the hardware and software, which was insufficiently robust in the early stages of phase 1 to capture a high proportion of shocks). The remaining 30 subjects constituted the group retained for phase 1 analysis. This high recruitment attrition rate reflected a relatively high incidence of equipment issues early in the study, as well as administrative difficulties in reporting X-rays. The final group of 30 subjects had an average (± 2 standard deviations) of 2473 $\pm$ 1204 shocks administered during treatment using the Storz Modulith. Energy settings from 1–6 were used.

A total of 85 patients were recruited to phase 2, of

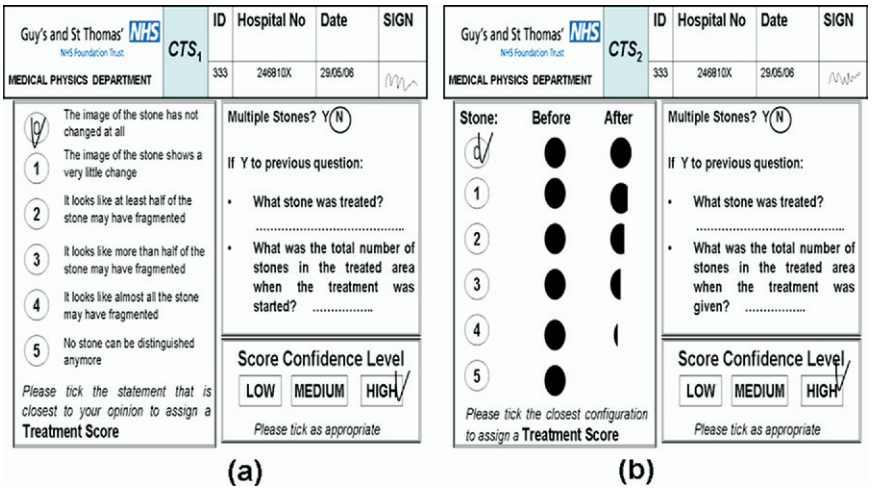

Fig. 8. The forms used to obtain treatment scores from the clinicians. Panel (a) shows the form used by the radiologist to give CTS_1 at the end of the therapy. Panel (b) is the form used to obtain CTS_2 from the consultant urologist at the follow-up several weeks after therapy (and was used as the gold standard). Both forms show simulated examples of the evaluation of a treatment, which had no effect on the stone size (*i.e.*, the data does not refer to a real patient, and the signatures are simulations). The form asks for treatment details, ID and DATE (which are the same as those saved by the SEAC software), the patient hospital number (to be sure that the assessment was done on the correct patient) and information on whether the patient presented with a single stone or multiple stones. In cases of multiple stones, the operator is also asked to indicate on which stone treatment and assessment were performed, and to specify the number of stones in the treatment area (where the shocks were targeted). The form asks for the clinician who did the assessment to provide a signature (SIGN), and also to assign a "score confidence level". In the cases where this score was low, two independent experts were requested to assign a treatment score. Except in the case of two patients for phase 2, where zero fragmentation was assessed consistently by both experts for CTS_2, all treatments with a low confidence level were discarded from the analysis.

which 49 satisfied the two conditions required for their acoustic data to be included in the trial: first, a complete clinical follow-up at three weeks was available; and, second, the recorded sequences for each patient represented at least 30% of shocks given to that patient during the treatment session. The attrition rate in phase 2 was considerably better than in phase 1 because of improved experience with the PAS. To be specific, treatment was not tolerated by three patients, no follow-up was available for 16 patients and in a further two cases, the X-rays were of poor quality and could not be interpreted (see caption to Fig. 8). The equipment was damaged for 15 cases.

The average number of shocks administered in the phase 2 group was similar to that in phase 1, at 2461 $\pm$ 1160. Energy settings from 1–6 were used. The operators favored setting 4 for the majority of treatments in both phases 1 and 2, although some variation occurred in all cases at the start and after realignment of the stone, and in some cases higher settings were used.

Two forms were devised to allow clinicians to quantify their judgment of the treatment (Fig. 8). These provided a six-point scale of clinical treatment scores (0 to 5) based on the degree of stone fragmentation (and made without knowledge of the PAS output). They were qualitatively judged by the lithotripter operator, from the X-ray at the end of the treatment (CTS_1) and at the three-week follow-up appointment (CTS_2) as judged by a urologist, with "0" indicating no fragmentation, "3" indicating 50% fragmentation and "5" complete fragmentation. The CTS_2 score was taken to be the gold standard because the clinical decision on the need for further treatment was based on this. The initial clinical score (CTS_1) was just a "look-see" and had no influence on any clinical decisions regarding the need for retreatment. The *in vitro*–derived "rules" for discriminating "effective" shocks were adjusted in the light of phase 1 clinical data to maximize the level of agreement between CTS_2 and the PAS output in the form of the parameter TS_0 (the percentage of shocks classified by the rules as "effective"). The clinically adjusted rules for defining an effective shock were programmed into the SEAC software and the system performance was then examined in the phase 2 study.

In phase 2, the SEAC software was adapted to provide two outputs designed to have a clinical relevance: a real-time indicator giving a binary classification of each shock as effective or ineffective, and a global figure of merit, or treatment score, based on the percentage of effective shocks relative to the total number ad-

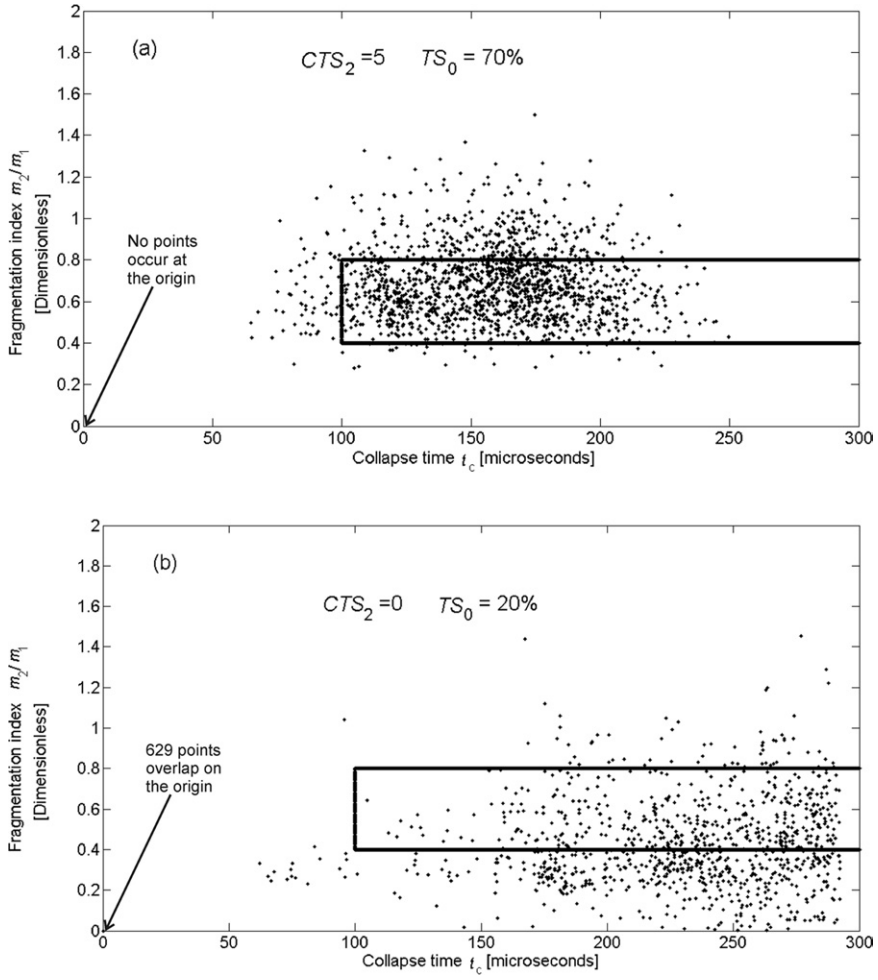

Fig. 9. Plots from phase 1 of the clinical study, giving the values of the acoustic parameters m_2/m_1 and t_c for each shock from two sample treatments. The first plot (a) is for a successful treatment and the second plot (b) is for an unsuccessful treatment as classified by the clinician from the X-rays (CTS_2). The area delimited by the solid line ($0.4 < m_2/m_1 < 0.8$ and $t_c > 100$ μs) represents the semi-empirical rules that appear from the phase 1 study to give the optimum indication of effective and ineffective shocks. It is postulated from the phase 1 study that a large number of effective shocks (*i.e.*, falling within the solid lines) result in a successful treatment. The number of signals where the analysis allocated values of $t_c = 0$ and $m_2 = 0$ were zero and 629 in Fig. 9, a and b, respectively.

ministered, TS_0. To assess the usefulness of TS_0 as a predictor of the degree of success of a treatment, it was compared in phase 2 with the two clinical treatment scores, CTS_1 and CTS_2 (both of which were made in ignorance of TS_0).

RESULTS

Phase 1 clinical study

Figure 9 plots m_2/m_1 against t_c for two separate phase 1 treatments. It was established early on that use of the ratio of the acoustic parameters m_1 and m_2 was a valuable way of removing interpatient variation in the absolute values of each parameter. This variation was because of differences in acoustic path length in tissue from the focus to the sensor. Each point on the plot represents the acoustic parameters for a single shock. Figure 9a is for a treatment in which the clinical score $CTS_2 = 5$, *i.e.*, a successful treatment. The total number of points is 2,231, which represents the 74% sample of shocks obtained using the SEAC software from this study (the missing shocks occurred at the start of the treatment and immediately after realignment, when the lithotripter energy settings were lower than those used for the majority of the treatment, as described in the Discussion). There were no recorded signals with $t_c = 0$ and $m_2 = 0$ in this case. Figure 9b is the corresponding plot for an unsuccessful treatment ($CTS_2 = 0$). In this case, the plot contains data for a sample of 2,185 shocks,

or 87% of the total treatment, of which (in stark contrast to Fig. 9a) a total of 629 signals were classified with t_c = 0 and m_2 = 0. The clustering of acoustic data points is different visually between the two treatments, with greater dispersion of points in the unsuccessful treatment and with wider ranges of both m_2/m_1 and t_c. Values of t_c are, in both cases, well below those seen *in vitro* (t_c~300 μs) as found in previous studies (Cunningham et al. 2002; Zhong et al. 1997).

It was decided, on the basis of the clinical data from phase 1, to alter the *in vitro* rules such that an effective shock is defined as one in which both $0.40 < m_2/m_1 < 0.8$ and $t_c > 100$ μs. These rules define a region shown as a box in Fig. 9, a and b. The upper limit of 0.8 on the ratio m_2/m_1 for effective shocks was imposed to eliminate shocks that generated signals close to the noise level where the algorithm tended to return large values of this ratio. A noisy acoustic signal is, by implication, interpreted here as one in which there is minimal scattered or emitted signal owing to lack of targeting, resulting in an ineffective shock. No upper limit was placed on t_c, although it is possible that values of t_c above 250 μs may be an artefact of the burst detection algorithm in noisy data. The lower limit on t_c is imposed because this is a clear indicator (to the operator) that the shock is weak and probably ineffective. Such was the ability of the instantaneous value of t_c to discriminate between an effective or ineffective shock (especially when it was combined with the m_2/m_1 information) that it was not necessary to exploit other useful outputs from the device (such as the trend and variability in the value of t_c, available in the lower right of Fig. 7, which could potentially add discrimination).

A measure of the treatment score TS_0 provided by the acoustic system was defined using the rules as the ratio of effective shocks to the total sample size expressed as a percentage. This TS_0 value is closely related to the total number of effective shocks in a 3,000-shock treatment. In Fig. 9, a and b, the values of TS_0 can be calculated to be 70% and 20%, respectively. Figure 10, a and b, presents the overall clinical results on the 30 subjects included in phase 1. These are plots of the three-week follow-up appointment score CTS_2, compared with the treatment score from the clinicians viewing the X-rays immediately after treatment, CTS_1 (Fig. 10a), and the treatment score from the device TS_0 (Fig. 10b). The dotted lines have been added to indicate the threshold levels of the treatment scores that have been selected to generate a binary scoring system from the continuous TS_0 score and the digitized clinical scores, CTS_1 and CTS_2. For both of the clinical scores, this threshold was placed such that values lower than 3 were considered unsuccessful treatments and values of ≥3 were considered successful treatments. This approach was suggested by the distribution of clinical scores, with clinicians favoring the

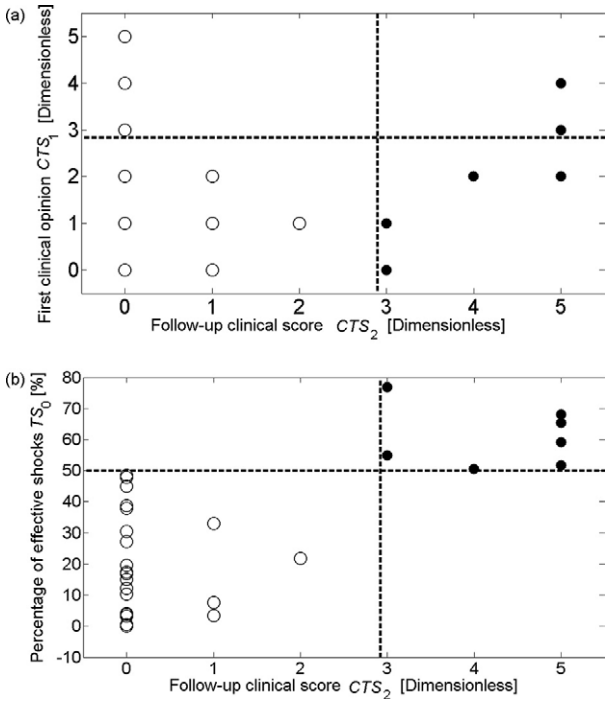

Fig. 10. Phase 1 clinical study results. In the first plot (a), the initial clinical treatment score, CTS_1, is compared with the clinical treatment score obtained at the three-week follow-up assessment, CTS_2. In the second plot (b), the treatment score from the SEAC system, TS_0, is compared with CTS_2. Each point represents the result obtained from a single treatment of 2473 ± 1204 shocks. The solid circles indicate successful treatments (*i.e.*, $CTS_2 \geq 3$) and the open circles indicate unsuccessful treatments (*i.e.*, $CTS_2 < 3$). The second plot (b) indicates that successful treatments, as classified at the follow-up (*i.e.*, $CTS_2 \geq 3$), have high values of TS_0. It is postulated from this phase 1 clinical study that scores of $TS_0 \geq 50\%$ can be usefully classified as successful. The dotted lines indicate the position of these thresholds determined from phase 1. Both graphs include 30 points, with fewer being visible because of overlapping; for example in (a), 11 patients score $CTS_1 = CTS_2 = 0$, two patients score $CTS_1 = 3$ with $CTS_2 = 5$ and four patients score $CTS_1 = 1$ with $CTS_2 = 0$.

two extreme values 0 and 5, with relatively few intermediate values selected. The filled circles in Fig. 10 indicate successful treatments where CTS_2 is ≥3, and the open circles indicate the unsuccessful treatments ($CTS_2 < 3$). The TS_0 threshold, on the other hand, was selected by calculating the kappa statistic (Viera and Garrett 2005) for a range of thresholds and choosing the threshold with the highest kappa value. The kappa statistic is used widely for quantifying inter-observer agreement in radiographic interpretations. In this case, the comparison considers the PAS device to represent one of the observers (and its output to represent the corresponding observation), and it considers the clinician viewing the X-ray to be the second observer. The TS_0 threshold was selected from the device comparison with the gold standard score CTS_2 (Fig. 10b). In this case,

the maximum value of kappa is 0.95 at $TS_0 = 50\%$. By applying this threshold to the data, values of $TS_0 < 50\%$ are considered to be unsuccessful treatments and values of $\geq 50\%$ are considered to be successful. This threshold was incorporated into the SEAC software and used in the phase 2 clinical study. Applying this threshold to the phase 1 data for CTS_1 generates a kappa = 0.32, which indicates a considerably lower level of agreement between the score provided by the acoustic system (TS_0) and the clinical observation made immediately after treatment (CTS_1) compared with the agreement found between the PAS device and CTS_2, the gold standard clinical score. The same poor level of agreement (kappa = 0.32) is found between CTS_1 and CTS_2 (Fig. 10a) for the phase 1 data. Phase 1, therefore, indicates the unreliability of CTS_1 and greater reliability of TS_0, as judged against the gold standard of CTS_2. Although the CFD and *in vitro* studies moderate the circularity of this argument to some extent, it is to remove that circularity entirely that the phase 2 study was set up.

Phase 2 clinical study

The results of phase 2 are shown in Fig. 11, a and b. As for phase 1, these plots compare the PAS system and clinical treatment scores (for 49 subjects in this case). The dotted lines show the thresholds for the treatment scores that provide a binary classification of successful and unsuccessful treatments. As before, the solid circles indicate the successful treatments, where CTS_2 is ≥ 3, and the open circles indicate the unsuccessful treatments ($CTS_2 < 3$). From Fig. 11a it is clear that degree of agreement between the two clinical scores CTS_1 and CTS_2 is similar to that found in phase 1. This level of agreement is quantified in this case by kappa = 0.38. A similar level of agreement (kappa = 0.42) is found between the output of the PAS system (TS_0) and CTS_1. However, in Fig. 11b it can be seen that the level of agreement between the PAS device and the gold standard CTS_2 remains good, in this case with kappa = 0.94. The sensitivity of the PAS in correctly categorizing the treatment success is 91.7%, with 11 individuals identified as having a TS_0 of $\geq 50\%$ compared with 12 individuals having a CTS_2 of ≥ 3. The specificity of the PAS and SEAC system in this context was 100% with all 37 individuals with $CTS_2 < 3$ identified by the device as having unsuccessful treatments.

Variability as a result of respiration

The power spectral density of a 5-min clinically-acquired trace of m_1 is shown in Fig. 12. This shows a lobe that is attributed to the 0.3-Hz respiration frequency of the patient. The trace of m_1 itself is shown as an inset to Fig. 12. The depth of respiration can be estimated from the relative amplitude of the respiratory lobe. The results from both clinical studies (phases 1 and 2) were pooled to examine the level of agreement between the

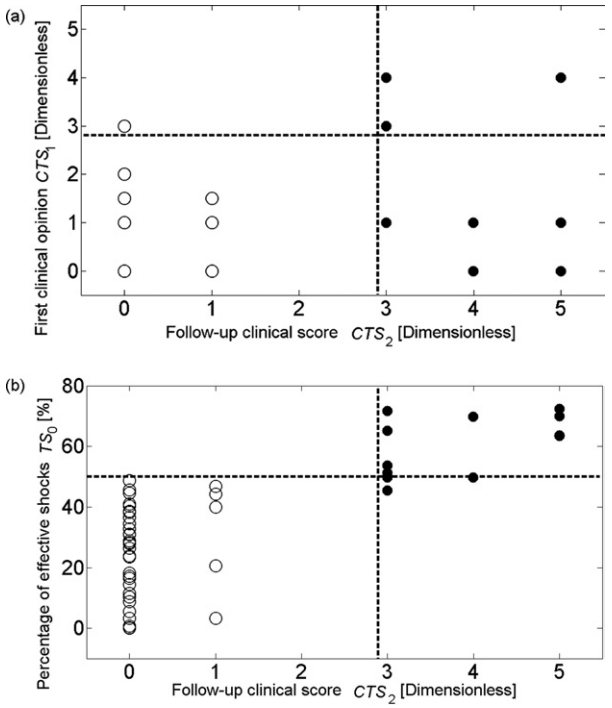

Fig. 11. Phase 2 clinical study results. In the first plot (a), the initial clinical treatment score, CTS_1, is compared with the clinical treatment score obtained at the three-week follow-up assessment, CTS_2. In the second plot (b), the treatment score from the SEAC system, TS_0, is compared with CTS_2. Each point represents the result obtained from a single treatment of 2461 ± 1160 shocks. The solid circles indicate successful treatments (*i.e.*, $CTS_2 \geq 3$) and the open circles indicate unsuccessful treatments (*i.e.*, $CTS_2 < 3$). In the first plot (a), the initial clinical assessment differs significantly from that at follow-up. In the second plot (b), the SEAC system gives a significant agreement with the clinical results determined at follow-up. The dotted lines indicate the position of these thresholds determined from phase 1. Both graphs include 49 points, although (as with Fig. 10) some overlapping occurs; for example in (a), 18 patients score $CTS_1 = CTS_2 = 0$; two patients score $CTS_1 = 4$, $CTS_2 = 5$; four patients score $CTS_1 = 1$ with $CTS_2 = 3$; three patients score $CTS_1 = 2$ with $CTS_2 = 0$; nine patients score $CTS_1 = 1$ with $CTS_2 = 0$; and three patients score $CTS_1 = 1$ with $CTS_2 = 1$.

observation of an ineffective treatment (defined using CTS_2) with that arrived at if an ineffective treatment is defined as being one for which the detected respiratory lobe exceeds some threshold amplitude. The kappa value for the case when the respiratory lobe threshold is set at 50% is 0.35, indicating that a measure of respiratory depth alone using the device has some clinical use, in that deep respiration may degrade targeting.

Figure 13 shows that deep breathing (represented by a high value of relative PSD) corresponds, not surprisingly, to relatively poor targeting (where $t_c \leq 100$ μs), whereas shallow breathing (represented by a low value

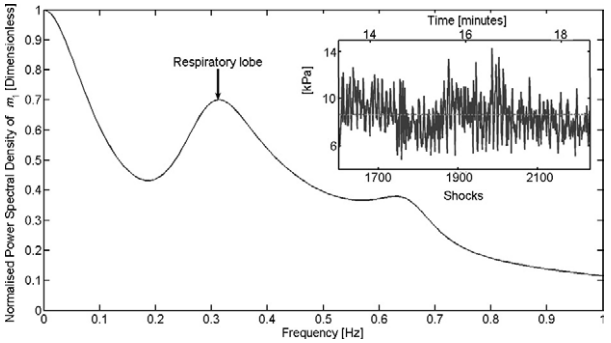

Fig. 12. The PSD (normalized such that the peak value is unity) of a sample trace of the acoustic parameter m_1. The trace of m_1 is shown as an inset. The average value of m_1 is ~8.6 kPa (dotted line). A respiratory lobe occurs in the PSD at ~0.3 Hz. This corresponds with the recorded respiration rate of the patient and suggests that the SEAC system is capable of detecting stone motion caused by respiration. The shocks were administered with a rate of 120 shocks per minute.

of relative PSD) corresponds to relatively good targeting ($t_c > 100$ μs).

DISCUSSION

The PAS and the associated clinical analysis (SEAC) software have been demonstrated in this study to provide clinically relevant real-time feedback to the operator that relates to the targeting of the stone and the effectiveness of the shocks delivered to date. Furthermore, once a statistically significant number of shocks have been delivered, it can (through $TS(t)$, which becomes TS_0 at the end of the treatment) indicate the degree of fragmentation achieved once a substantial part of the procedure has been completed. In particular, the concept of an effective shock has been defined in terms of measurable acoustic parameters that themselves have been shown to relate to targeting accuracy and the degree of fragmentation generated. As the associated web page movie shows (see footnote on first page of this article), the device uses a red-green indicator to provide shock-by-shock real-time feedback of the effectiveness of each shock (as well as other indicators as listed in the caption of Fig. 7), which might in the future be used to adjust treatment in real time. Instead of checking targeting at preset times during X-rays, for example (which, if it occurs before targeting has degraded, constitutes an unnecessary X-ray exposure and, if it occurs many shocks after targeting was degraded, constitutes an unnecessary exposure to ineffective shocks), the operator could be alerted to the requirement to check targeting by a sequence of consecutive ineffective shocks (as shown by a persistent red indicator light, or by the trends in the graphs at the bottom right of Fig. 7). However, for this paper the ethics approval did not allow the lithotripter operator to alter the treatment in any way as a result of the PAS data, so that the statistical testing was based on the proportion of shocks that were effective, a treatment score TS_0 that was delivered only at the end of the treatment. The phase 2 study results confirm almost perfect agreement (kappa = 0.94) between the number of effective shocks administered in a typical ESWL treatment and the assessment of the degree of stone fragmentation identified by the clinician three weeks after treatment on the basis of X-rays. This result supports the hypothesis that the acoustic parameters that were selected have some clinical relevance in ESWL. The precise clinical interpretation of the acoustic parameters is not fully explored here, and does not need to be unconditionally categorized to demonstrate (through the correlation of acoustic and clinical data) the utility of the PAS. Indeed, because of the complexities of the tissue/stone/shock/cavitation interactions that can be expected to occur *in vivo*, neither the underlying model, nor the hypotheses as to the cause of the signal characteristics, will capture all aspects of the interaction. However, as expected from *in vitro* studies and CFD modeling, the signal varies with targeting and with the degree of stone fragmentation to an extent that is clinically useful.

One limitation of the study is that about 20% of shocks have been excluded from the analysis. These occur at the very start of the treatment and immediately after relocation of the stone on X-ray and will therefore tend to be at lower energy settings than those used for the majority of the treatment. This omission will make the device-derived treatment score, TS_0, higher than it would be if more of these (probably) ineffective shocks had been included. This

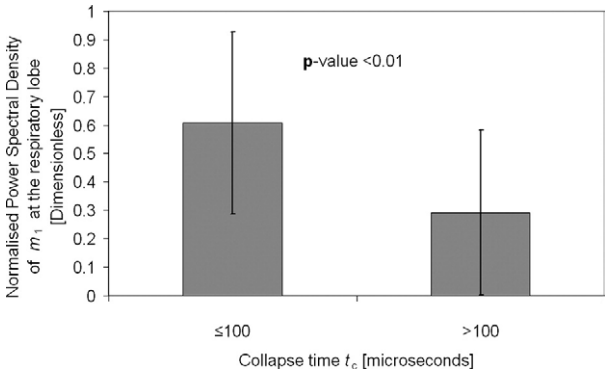

Fig. 13. Comparison of the average amplitude of the normalized PSD of m_1 at the lobe attributed to respiration (see Fig. 12) in treatments with t_c below and above the threshold of 100 μs. This graph shows that deep breathing, represented by a high value of relative PSD, corresponds with relatively poor targeting (where $t_c \leq 100$ μs), whereas shallow breathing, low PSD, corresponds with relatively good targeting ($t_c > 100$ μs). There is a significant difference between the two cases (**p**-value < 0.01).

problem arises because the system requires manual entry of the shockwave energy setting. Manual entry is easy for the majority of the shocks where the setting is fixed, but can be difficult for shocks where the setting is being stepped up or down by the operator. Clearly, if the PAS/SEAC system were incorporated into the construction of the lithotripter, this limitation might be designed out by allowing automated capture of the setting.

The key clinical value of the PAS and SEAC software may lie less in their ability to predict the efficacy of the completed treatment, and more in assisting the operator to make decisions during ESWL concerning the ongoing effectiveness of the treatment, in terms of both the targeting and the likelihood of stone fragmentation. The targeting information provided by the device will clearly be of less value in lithotripters with particularly large focal zones, where precise targeting is not critical (Eisenmenger et al. 2002). In these cases, the system can still provide information on the effectiveness of stone fragmentation that may prove to be clinically valuable.

Currently, lithotripter operators have little feedback on these critical treatment success factors other than that provided during periodic realignment of the stone under imaging control. The present system serves to inform the operator so that they can ensure that the maximum number of shocks delivered is effective and limit the number of ineffective shocks that contribute only to the morbidity of the treatment. The hypothesis that depth of respiration could affect the clinical outcome is not new (Warner et al. 1989; Cleveland et al. 2004), but this paper does demonstrate *in vivo* the sensitivity of the PAS to factors that influence targeting. The finding also supports the physical interpretation of the acoustic parameter, m_1, as being an indicator of targeting. The ability of the PAS to detect respiration-driven movement of the stone in and out of the shockwave focus (Fig. 12; Fedele 2008) means that the device could be used to provide a respiratory gating signal for shockwave release.

The system described would be particularly valuable if it could reduce the retreatment rate seen in ESWL, and lower the consequent morbidity and cost. Although the operator may be able to obtain a good prediction of the likelihood of success of the treatment using the present system, a further clinical study (with commensurate ethics approval for this endpoint) would be required to show whether the passive acoustic information could be used in some manner to reduce retreatment rates in ESWL.

Acknowledgments—The Engineering and Physical Sciences Research Council provided a grant from 2000–2003 (EPSRC grant, GR/N19243/01; principle investigator: T.G. Leighton; co-investigator: A.J. Coleman), which was followed by a further grant from 2005–2006 (Grant ref: EP/D503310/1; principle investigator: T.G. Leighton; co-investigator: A.J. Coleman). T. Gill and D. Bell (Precision Acoustics Ltd.) provided invaluable assistance in developing the passive sensor. R. Tiptaft, J. Glass, D. Phillips and T. Jessop (Urology Department at Guy's and St. Thomas' NHS Trust) are gratefully acknowledged for their support during the clinical study. C. McKinnon (Centre for Enterprise and Innovation, University of Southampton) and T. Parlett (Intellectual Property Officer, Guy's & St. Thomas' NHS Trust) are thanked for their work in the contractual and commercial aspects of this study. From ISVR, D. Finfer is thanked for assistance in software programming, G. T. Yim is thanked for his advice on computing hardware and V. Humphrey is thanked for loan of interim replacement transducers and preamplifiers (and advice on the repair and testing) when the apparatus was sent for servicing. All clinical work was approved by the local research ethics committee of Guy's and St. Thomas' NHS Foundation Trust.

REFERENCES

Auge BK, Preminger GM. Update on shock wave lithotripsy technology. Curr Opin Urol 2002;12(4):287–290.

Bailey MR, Pishchalnikov YA, Sapozhnikov OA, Cleveland RO, McAteer JA, Miller NA, Pishchalnikova IV, Connors BA, Crum LA, Evan AP. Cavitation detection during shock-wave lithotripsy. Ultrasound Med Biol 2005;31(9):1245–1256.

Blake JR, Hooton MC, Robinson PB, Tong RP. Collapsing cavities, toroidal bubbles and jet impact. Phil Trans Royal Soc Lond A 1997;355:537–550.

Chaussy C, Schmiedt E. Shock wave treatment for stones in the upper urinary tract. J Urol Clin North Am 1983;10(4):743–750.

Chitnis PV, Cleveland RO. Quantitative measurements of acoustic emissions from cavitation at the surface of a stone in response to a lithotripter shock wave. J Acoust Soc Am 2006;119(4):1929–1932.

Cleveland RO, Lifshitz DA, Connors BA, Evan AP, Willis LR, Crum LA. In vivo pressure measurements of lithotripsy shock waves in pigs. Ultrasound Med Biol 1998;24(2):293–306.

Cleveland RO, Sapozhnikov OA, Bailey MR, Crum LA. A dual passive cavitation detector for localized detection of lithotripsy-induced cavitation *in vitro.* J Acoust Soc Am 2000;107(3):1745–1758.

Cleveland RO, Anglade R, Babayan RK. Effect of stone motion on *in vitro* comminution efficiency of a Storx Modulith SLX. J Endourol 2004;18(7):629–633.

Cleveland RO, Sapozhnikov OA. Modeling elastic wave propagation in kidney stones with application to shock wave lithotripsy. J Acoust Soc Am 2005;118:2667–2676.

Coleman AJ, Choi MJ, Saunders JE, Leighton TG. Acoustic emission and sonoluminescence due to cavitation at the beam focus of an electrohydraulic shock wave lithotripter. Ultrasound Med Biol 1992;18:267–281.

Coleman AJ, Whitlock M, Leighton TG, Saunders JE. The spatial distribution of cavitation induced acoustic emission, sonoluminescence and cell lysis in the field of a shock wave lithotripter. Phys Med Biol 1993;38(11):1545–1560.

Cunningham KB, Coleman AJ, Leighton TG, White PR. Characterising *in vivo* acoustic cavitation during lithotripsy with time-frequency methods. Acoust Bull 2002;26(5):10–16.

Delakas D, Karyotis I, Daskalopoulos G, Lianos E, Mavromanolakis E. Independent predictors of failure of shockwave lithotripsy for ureteral stones employing a second-generation lithotripter. J Endourol 2003;17(4):201–205.

Ding Z, Graceswki SM. The behaviour of a gas cavity impacted by a weak or strong shock wave. J Fluid Mech 1996;309:183–209.

Eisenmenger W, Du XX, Tang C, Zhao S, Wang Y, Rong F, Dai D, Guan M, Qi A. The first clinical results of "wide-focus and low-pressure" ESWL. Ultrasound Med Biol 2002;28(6):769–774.

Fedele F, Coleman AJ, Leighton TG. Use of cylindrical PVdF hydrophone in a study of cavitation adjacent to stone phantoms during extracorporeal shockwave lithotripsy. Proceedings of the IPEM Annual Scientific Meeting. Bath, United Kingdom, 2003.

Fedele F, Coleman AJ, Leighton TG, White PR, Hurrell AM. A new sensor for detecting & characterising acoustic cavitation in vivo during ESWL. Proc Inst Acoust 2004a;26(1):422–432.

Fedele F, Coleman AJ, Leighton TG, White PR, Hurrell AM. A new diagnostic sensor for extracorporeal shockwave lithotripsy. Acoust Bull 2004b:34–39.

Fedele F, Coleman AJ, Leighton TG, White PR, Hurrell AM. Development of a new diagnostic device for extracorporeal shockwave lithotripsy. Proceedings of the X Mediterranean Conference on Medical and Biological Engineering, "Health in the Information Society," 31 July-5 August 2004. IFMBE Proc 2004c;6:paper no. 54.

Fedele F, Coleman AJ, Leighton TG, White PR, Hurrell AM. Development of a new diagnostic sensor for extracorporeal shockwave lithotripsy. Proceedings of the First Conference in Advanced Metrology for Ultrasound in Medicine. J Phys Conf Series 2004d;1: 134–139.

Fedele F. Acoustic sensing of renal stones fragmentation in extracorporeal shockwave lithotripsy. PhD Thesis, University of Southampton 2008 (submitted).

Fong SW, Klaseboer E, Turangan CK, Khoo BC, Hung KC. Numerical analysis of a gas bubble near bio-materials in an ultrasound field. Ultrasound Med Biol 2006;32:925–942.

Gomha MA, Sheir KZ, Showky S, Abdel-Khalek M, Mokhtar AA, Madbouly K. Can we improve the prediction of stone-free status after extracorporeal shock wave lithotripsy for ureteral stones? A neural network or statistical model? J Urol 2004;172(1):175–179.

IEC. Medical Electrical Equipment–Part 1. General Requirement for Safety. IEC 60601–1. Geneva, Switzerland: International Electrotechnical Commission, 1988.

Klaseboer E, Turangan CK, Fong SW, Liu TG, Hung KC, Khoo BC. Simulations of pressure-pulse bubble interaction using boundary element method. Comput Methods Appl Eng 2006;195:4287–4302.

Leighton TG. The Acoustic Bubble. London: Academic Press, 1994.

Leighton TG, Cox BT, Phelps AD. The Rayleigh-like collapse of a conical bubble. J Acoust Soc Am 2000;107(1):130–142.

Leighton TG. From seas to surgeries, from babbling brooks to baby scans: The acoustics of gas bubbles in liquids. Int J Modern Phys B 2004;18(25):3267–3314.

Leighton TG, Coleman AJ, Fedele F, White PR. A passive acoustic system for evaluating the in-vivo performance of extracorporeal shockwave lithotripsy. 2004 UK; patent num. 0319863.7.

Leighton TG, Birkin PR, Hodnett M, Zeqiri B, Power JF, Price GJ, Mason T, Plattes M, Dezhkunov N, Coleman AJ. Characterisation of measures of reference acoustic cavitation (COMORAC): An experimental feasibility trial. In Doinikov AA, editor: Bubble and Particle Dynamics in Acoustic Fields: Modern Trends and Applications. Kerala: Research Signpost, 2005:37–94.

Leighton TG. What is ultrasound? Progr Biophys Mol Biol 2007;93(1–3):3–83.

Lingeman JE, Newman DM, Mertz HHO, Mosbaugh PhG, Steele RE, Knapp PM, Shirell W. Management of upper ureteral calculi with ESWL. IV World Congress on Endurology and ESWL, Madrid, Spain, 1986.

Madaan S, Joyce AD. Limitations of extracorporeal shock wave lithotripsy. Curr Opin Urol 2007;17(2):109–113.

Matula TJ, Hilmo PR, Bailey MR, Crum LA. In vitro sonoluminescence and sonochemistry studies with an electrohydraulic shockwave lithotripter. Ultrasound Med Biol 2002;28(9):1199–1207.

Owen NR, Bailey MR, Crum LA, Sapozhnikov OA, Trusov LA. The use of resonant scattering to identify stone fracture in shock wave lithotripsy. J Acoust Soc Am 2007;121:EL41–EL46.

Papadoukakis S, Stolzenburg J, Truss MC. Treatment strategies of ureteral stones. EAU-EBU Update Series 2006;4(5):184–190.

Papoulis A, Pillai SU. Probability, Random Variables and Stochastic Processes. 4th ed. Singapore: McGraw-Hill, 2001.

Pishchalnikov YA, Sapozhnikov OA, Bailey MR, Williams JC, Cleveland RO, Colonius T, Crum LA, Evan AP, McAteer JA. Cavitation bubble cluster activity in the breakage of kidney stones by lithotripter shockwaves. J Endourol 2003;17(7):435–446.

Sandilos P, Tsalafoutas I, Koutsokalis G, Karaiskos P, Georgiou E, Yakoumakis E, Vlahos L. Radiation doses to patients from extracorporeal shock wave lithotripsy. Health Phys 2006;90(6): 583–587.

Schmitt RM, Wuster H, Kraus W, Bibinger M. The effects of errors in positioning lithotripter and imaging kidney stones ultrasound. Proceedings of the Annual International Conference of the IEEE Engineering in Medicine and Biology Society 1990;12(1):252–253.

Skolarikos A, Alivizaos G, de la Rosette J. Extracorporeal shock wave lithotripsy 25 years later: Complications and their prevention. Eur Urol 2006;50(5):981–990.

Tan YM, Yip SK, Chong TW, Wong MY, Cheng C, Foo KT. Clinical experience and results of ESWL treatment of 3,093 urinary calculi with the Storz Modulith SL 20 lithotripter at the Singapore general hospital. Scand J Urol Nephrol 2002;36(5):363–367.

Tolley DA, Downey P. Current advances in shock wave lithotripsy. Curr Opin Urol 1999;9(4):319–323.

Turangan CK, Jamaluddin AR, Ball GJ, Leighton TG. Free-Lagrange simulations of the expansion and jetting collapse of air bubbles in water. J Fluid Mech 2008;598:1–25.

Viera AJ, Garrett JM. Understanding Interobserver Agreement: The Kappa Statistic. Farm Med 2005;37(5):360–363.

Warner MA, Warner ME, Buck CF, Segura JW. Clinical efficacy of high frequency jet ventilation during extracorporeal shock wave lithotripsy of renal and ureteral calculi: A comparison with conventional mechanical ventilation. J Urol 1988;139(3):486–487.

Xi X, Zhong P. Improvement of stone fragmentation during shock-wave lithotripsy using a combined EH/PEAA shock-wave generator-in vitro experiments. Ultrasound Med Biol 2000;26(3):457–467.

Xi X, Zhong P. Dynamic photoelastic study of the transient stress field in solids during shock wave lithotripsy. J Acoust Soc. Am 2001; 109(3):1226–1239.

Xu Z, Hall TL, Fowlkes JB, Cain CA. Effects of acoustic parameters on bubble cloud dynamics in ultrasound tissue erosion (histotripsy). J Acoust Soc Am 2007;122(1):229–236.

Zhong P, Chuong CJ, Preminger GM. Propagation of shock waves in elastic solids caused by cavitation microjet impact. II: Application in extracorporeal shock wave lithotripsy. J Acoust Soc Am 1993; 94(1):29–36.

Zhong P, Cioanta I, Cocks FH, Preminger GM. Inertial cavitation and associated acoustic emission produced during electrohydraulic shock wave lithotripsy. J Acoust Soc Am 1997;101(1):2940–2950.

Zhong P, Zhou Y. Suppression of large intraluminal bubble expansion in shock wave lithotripsy without compromising stone comminution: Methodology and in vitro experiments. J Acoust Soc Am 2001;110(6):3283–3291.

Zhu S, Cocks FH, Preminger GM, Zhong P. The role of stress waves and cavitation in stone comminution in shock wave lithotripsy. Ultrasound Med Biol 2002;28(5):661–671.

APPENDIX

SUPPLEMENTARY DATA

Supplementary data associated with this article can be found, in the online version, at doi:10.1016/j.ultrasmedbio.2008.03.011.

Video Clips cited in this article can also be found online at: http://www.umbjournal.org.